Infrared Physics and Technology 105 (2020) 103230

Contents lists available at ScienceDirect

Infrared Physics & Technology

journal homepage: www.elsevier.com/locate/infrared

Growth and mid-infrared luminescence property of Ho^{3+} doped CeF_3 single crystal

Yilun Yang[a,b], Lianhan Zhang[a], Shanming Li[a,b], Shulong Zhang[a,b], Yuhang Zhang[a,b], Qiannan Fang[a], Mingzhu He[a], Min Xu[a], Yin Hang[a,*]

[a] *Laboratory of Micro-Nano Optoelectronic Materials and Devices, Key Laboratory of Materials for High-Power Laser, Shanghai Institute of Optics and Fine Mechanics, Chinese Academy of Sciences, Shanghai 201800, China*

[b] *Center of Materials Science and Optoelectronics Engineering, University of Chinese Academy of Sciences, Beijing 100049, China*

ARTICLE INFO

Keywords:
CeF_3
Ho^{3+}

ABSTRACT

A Ho^{3+}-doped CeF_3 crystal was successfully grown for the first time using the Bridgman method, and its spectral properties were studied. By analyzing the absorption and emission measurements of the Ho:CeF_3 crystal with the Judd–Ofelt theory, the intensity parameters $\Omega_{2,4,6}$, emission cross-sections, gain cross-sections, and excited state lifetimes were calculated. It was found that the peak absorption cross-section around 447 nm is 0.4339×10^{-20} cm^2, which matched to the commercially available blue laser diode lasers. The 2.0 µm excitation emission of the Ho:CeF_3 crystal corresponding to the stimulated emission Ho^{3+}:$^5I_7 \rightarrow ^5I_8$ transition has an emission cross section of 0.24×10^{-20} cm^2 with FWHM of 146 nm.

1. Introduction

High power solid-state lasers in the eye-safe 2 µm regime is located in the strong absorption band of water, that make it attractive for a variety of scientific and technical applications including medical, spectroscopy, atmosphere monitoring, remote sensing and many other fields [1,2]. In addition, it can be used as pumping source for optical parametric oscillator (OPO) systems [3]. The main challenge with Ho^{3+} ions in mid-infrared lasers is the lack of suitable pump source of commercially available laser diode. To solve this problem, Tm^{3+} has been used as a sensitizer in many crystals to transfer the absorbed pumping energy into Ho^{3+} in the Tm^{3+}-Ho^{3+} co-doped system. However, the up-conversion effects and energy transferring process in co-doped system increase the laser threshold while reduces the laser efficiency. Hence, Ho^{3+} and Tm^{3+} doped in separate crystals can alleviate the above effects [4].

The efficient IR fluorescence required low phonon energy. The fluoride crystals have lower maximum phonon energy (about 400–560 cm^{-1}) than other crystals [5,6], which is beneficial for reduces nonradiative relaxation between adjacent energy levels. Compared with oxide crystals, fluoride crystals have many other advantages, such as easy-processing, lower reflective index and broadband transmittance [7,8,9]. In hexagonal fluoride crystals, CeF_3 is a crystal that has been reported less frequently. Compared with LaF_3 crystal, the ionic radius of Ce^{3+} is closer to that of rare-earth active ions, which can achieve higher concentration of doping. On the basis of the above reasons, we systematically studied the growth and spectral properties of Ho^{3+} doped CeF_3 single crystals.

In this work, we demonstrate the growth of 0.87 at.% Ho^{3+} doped CeF_3 single crystals by the Bridgman method, and its structures and spectroscopic properties were measured. The J-O theoretical calculations was used to analyze the absorption and fluorescence spectrum, three J-O intensity parameters and fluorescence emission cross-section were obtained by calculation.

2. Experiments

The 0.87 at.% Ho^{3+} doped CeF_3 crystal was grown by the Bridgman method. The CeF_3 (4 N) and HoF_3 (4 N) fluoride powder provided commercially have been used as raw materials. The raw material was charged into a graphite crucible having a diameter of 20 mm, and the melt in the crucible was melted in a high-temperature zone having a temperature of 1640 °C for 10 h. The crucible was then pulled to a low temperature zone at a speed of 1.2 mm/h and a speed of 5 rpm to drive the crystal growth process. Finally, the rystals were cooled to room temperature at a rate of 30 °C/h. In order to avoid interference of oxygen and water during crystal growth, the interior of the furnace is in a high-purity Ar (50%) and CF_4 (50%) atmosphere throughout the

* Corresponding author.
E-mail address: yhang@siom.ac.cn (Y. Hang).

https://doi.org/10.1016/j.infrared.2020.103230
Received 29 November 2019; Received in revised form 6 February 2020; Accepted 6 February 2020
Available online 07 February 2020

entire process. Finally, we obtained a Ho:CeF_3 single crystal with a size of Φ20 mm × 30 mm.

The as-grown crystal is oriented and a (1 1 1) -oriented sample is cut out for subsequent spectral testing. Crystal structure identification for crystal powder was under taken on a D/max 2550 X-ray diffraction (XRD) using Cu Kα radiation. The concentration of the Ho^{3+} ions in the CeF_3 crystal was measured by inductively coupled plasma atomic emission spectrometry (ICP-AES) analysis. The IR transmittance spectrum of Ho:CeF_3 crystal was recorded by a Nicolet 6700 FTIR spectrometer. The absorption spectrum in the range of 300–2200 nm was recorded by a Perkin Elmer Lambda 950 spectrometer. The fluorescence spectrum in range of 1800–2200 nm and fluorescence decay curve were recorded by an Edinburgh Instruments FLSP920 steady-state spectrometer under 450 nm LD excitation.

3. Results and discussions

3.1. Crystal growth results

The as-grown Ho:CeF_3 crystal was prepared successfully without any cracking. The doping concentrations of crystal sample for testing were measured to be 0.87 at.% of Ho^{3+} in Ho:CeF_3. The segregation coefficient of Ho^{3+} in the CeF_3 crystal are approximate 0.4. As shown in Fig. 1, the XRD pattern of the as-grown Ho:CeF_3 crystal is in good agreement with the standard CeF_3 (JCPDS 08-0045). This indicating that the crystal quality of Ho: CeF_3 grown by the Bridgman method is high. The lattice parameters of Ho:CeF_3 was calculated to be a = 0.7129 nm and c = 0.7285 nm, both very similar to pure CeF_3 single crystal (a = 0.7112 nm, c = 0.7279 nm).

3.2. Absorption properties and J–O analysis of Ho:CeF_3

The 2.5–25 μm room-temperature infrared transmission spectrum of the Ho:CeF3 crystal was shown in Fig. 2. There are two reasons for the infrared impermeability band at 2.5–6.5 μm: One of the reasons for is the 2.5–4 μm absorption band of residual OH^- groups in the fluoride crystal [10]. The other reason is $^2F_{7/2} \rightarrow {}^2F_{5/2}$ transition of Ce^{3+} [11].

The room-temperature absorption spectra in the range of 300–2200 nm of Ho:CeF3 crystal was shown as absorption cross-section in Fig. 3. There are 7 main absorption bands centered at around 414, 447, 534, 636, 858, 1142 and 1927 nm, which correspond to the transitions starting from the ground state $^5I_8$ to levels $^3G_5$, $^5G_6+{}^5F_1$, $^5F_4+{}^5S_2$, $^5F_5$, $^5I_5$, $^5I_6$ and $^5I_7$, respectively.

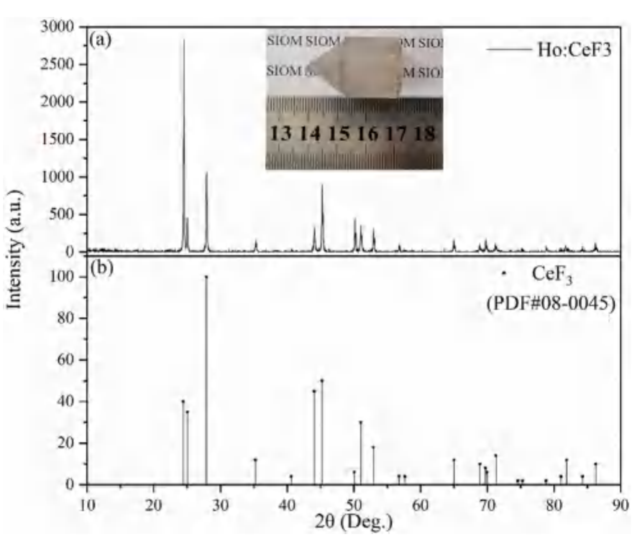

Fig. 1. The crystal sample and XRD pattern of CeF^3 crystals, (a) Ho:CeF_3 crystal and (b) CeF_3 crystal (JCPDS 08-0045).

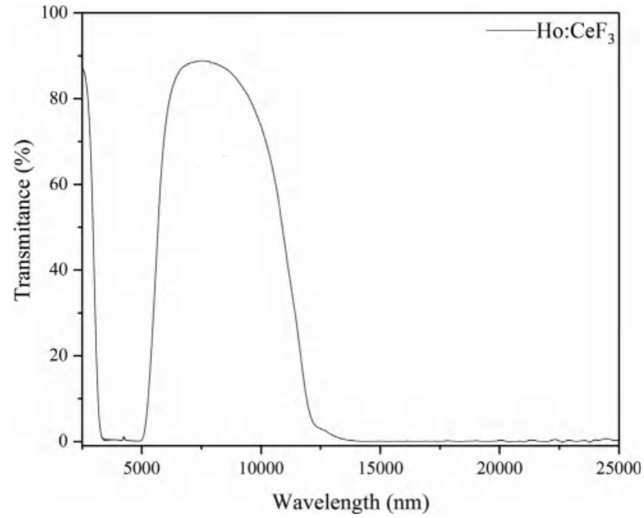

Fig. 2. Mid-far infrared transmittance spectrum of Ho:CeF_3 crystal.

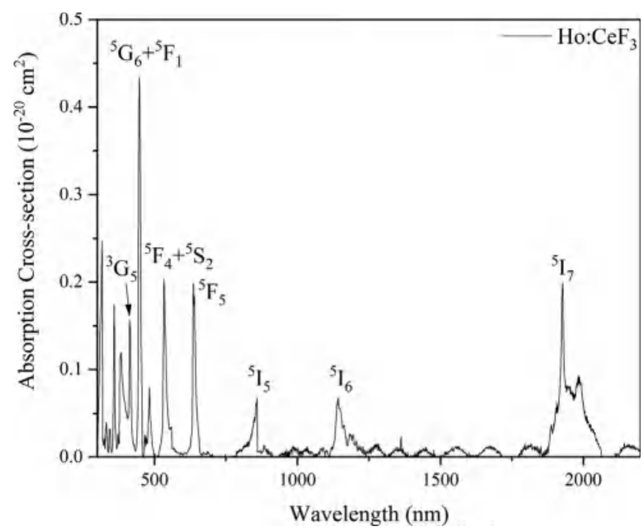

Fig. 3. Absorption cross-section of Ho:CeF_3 in the range of 300–2200 nm.

The absorption cross-section could be calculated from:

$$\sigma_{abs}(\lambda) = \frac{OD(\lambda)}{\log e \times L \times N_0} \tag{1}$$

where OD(λ) is the measured absorption optical density as a function of wavelength, L is the thickness of sample and N_0 is the number of Ho^{3+} ions per cm^3. The absorption cross-section of peak near 447 nm is 0.4339×10^{-20} cm^2, which adapts well to the commercially available blue laser diode (LD) lasers [12]. The absorption cross-section of peak around 1973 nm was 0.1992×10^{-20} cm^2 with FWHM of 126 nm, which can matches well to Tm^{3+}-doped laser crystal or fiber laser. On the other hand, the absorption of 0.0677×10^{-20} cm^2 has been observed at 1145 nm and turns out to be particularly suitable for 1150 nm LD or Raman laser pumping [13,14]. The central wavelengths of absorption peak, full band width at half-maximum (FWHM) and absorption cross-section are listed in Table 1.

The theory of Judd-Ofelt theory [15,16] has been applied to analyze the absorption spectrum of Ho:CeF_3 crystal and the intensity parameters $\Omega_{2,4,6}$ were calculated. The detailed calculation process of J-O analysis is described in the references. The refractive index of CeF_3 crystal used in the calculation is from calculated from Ref. [17], the reduced matrix element $\langle \|U^{(t)}\| \rangle$ is from Ref. [18]. Finally, experimental line strength S_{mea} and calculated line strength S_{cal} are also listed in

Table 1
Central wavelengths, peak absorption cross-sections, and measured and calculated line strengths of Ho:CeF$_3$ crystal.

$^5I_8$ to	λ (nm)	FWHM (nm)	σ_{abs} (10^{-20} cm^2)	S_{mea} (10^{-20} cm^2)	S_{cal} (10^{-20} cm^2)
$^5I_7$	1973	125.7	0.1992	0.6723	0.7011
$^5I_6$	1142	21.8	0.0677	0.1585	0.2049
$^5I_5$	859	7.1	0.0674	0.0459	0.0437
$^5F_5$	636	9.9	0.1983	0.4984	0.4777
$^5F_4+^5S_2$	534	10.1	0.2040	0.5992	0.4255
$^5F_1+^5G_6$	447	8.2	0.4339	0.9804	0.9792
$^3G_5$	414	6.3	0.1567	0.2304	0.2163

Table 1, and the three J-O intensity parameters were obtained: $\Omega_2 = 0.28 \times 10^{-20}$ cm^2, $\Omega_4 = 0.58 \times 10^{-20}$ cm^2 and $\Omega_6 = 0.40 \times 10^{-20}$ cm^2, respectively. The root-mean-square (RMS) deviation is 1.1520×10^{-21} cm^2, indicating the accuracy of the J-O intensity parameter for predicting the luminescent characteristics of Ho:CeF3 crystal. Furthermore, the calculated radiation lifetime τ_r for the excited state $^5I_7$ is 26.88 ms.

3.3. Emission properties of Ho:CeF$_3$ around 2 μm

The room temperature emission spectra ranging from 1800 to 2200 nm of Ho:CeF$_3$ crystal were measured under excited at 450 nm LD, shown as emission cross-section in Fig. 4. The emission cross-section can be calculated according to the Fuchtbauer-Ladenburg theory:

$$\sigma_{em} = \frac{\lambda^5 I(\lambda) A}{8\pi c \int n^2(\lambda)\lambda I(\lambda) d((\lambda)} \tag{6}$$

where A is the radiation transition rates, c is the speed of light, n(λ) is the is refractive index of light with wavelength λ in the crystal, and I(λ) refers to the measured fluorescence intensity at wavelength λ.

The Ho:CeF$_3$ crystal exhibits a wide emission band near 2 μm, corresponding to the radiative transitions of $^5I_7 \rightarrow {}^5I_8$ level which waveband centered at 1929 nm, 1988 nm and 2038 nm with full width at half width (FWHM) of 146 nm. The maximum peak emission cross section is 0.24×10^{-20} cm^2, located at 1988 nm.

Based on the above absorption and emission cross-section spectra, the gain cross-section $\sigma_G(\lambda)$ can be calculated by the following equation:

$$\sigma_G(\lambda) = P\sigma_{em}(\lambda) - (1-P)\sigma_{abs}(\lambda) \tag{7}$$

where the population inversion P is the ratio of the excited state $^5I_6$ level to total population of Ho^{3+} ions. The result of calculated gain

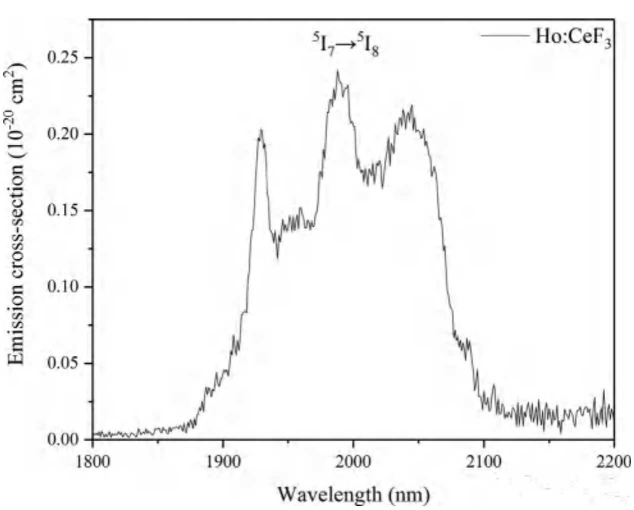

Fig. 4. Emission cross-section of Ho:$^5I_7 \rightarrow {}^5I_8$ transition in Ho:CeF$_3$ crystal.

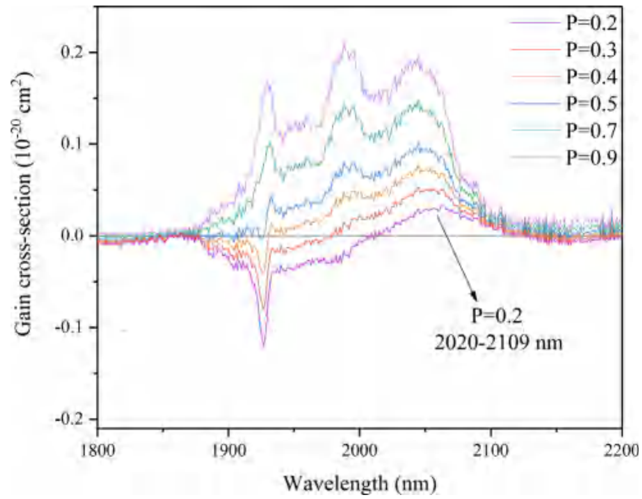

Fig. 5. Calculated gain cross-sections of Ho:$^5I_7 \rightarrow {}^5I_8$ transition in Ho:CeF$_3$ crystal.

cross-sections as a function of wavelength with different P values are shown in Fig. 5. The gain cross-section becomes positive from 2020 to 2109 nm once the population inversion level reaches 20%, which indicates a low pumping threshold for the Ho^{3+} 2.05 μm laser operations. When the inversion level is larger than 40%, the wavelength edge moves to the left of 1933 nm. At the inversion level of 70%, the gain cross-sections come to 0.10×10^{-20} cm^2 at 1932 nm and 0.15×10^{-20} cm^2 at 2045 nm, respectively.

3.4. Energy level lifetime of Ho^{3+}:$^5I_7$ energy level

To further investigate the 2 μm laser property of Ho:CeF$_3$, the fluorescence decay curve of the emission intensity at 2040 nm of $^5I_7$ level is recorded in Fig. 6. The fluorescence lifetime of Ho^{3+}:$^5I_7$ energy level is 45.45 μs, which is much lower than the calculation result 26.88 ms, and the quantum efficiency ($\eta = \tau_f/\tau_r$) reaches to 0.17%.

In order to eliminate the influence of the up-conversion process, different excitation bands were used for fluorescence lifetime testing. The measurements results of 450 nm LD, 533 nm xenon lamp and 640 nm LD excitation source measurements are very similar, 45.45, 43.18 and 48.89 μs, respectively. This proves that the reduction in the particles number of Ho^{3+}:$^5I_6$ level is not due to the up-conversion process. Therefore, it is necessary to discuss the energy transfer process of the energy level.

The involved energy transfer mechanisms of Ho^{3+} doped CeF$_3$ crystal are indicated in Fig. 6. In this crystal, there are two descending channels of the number of ions in the mid-infrared fluorescence emission. On the one hand, the energy is transferred from Ho^{3+}: $^5I_7$ level to the nearby Ce^{3+} in the ground state, and the Ce^{3+}: $^2F_{7/2}$ level is generated by the energy transfer (ET) process with the aid of the host phonons, this is the main reason for the reduction of Ho^{3+}:$^5I_7$ level lifetime. On the other hand, Ho^{3+} ions in the $^5I_6$ level can decay to the next lower level $^5I_7$ level through cross relaxation (CR) process (Ho^{3+}:$^5I_6$ + Ce^{3+}:$^2F_{5/2}$ → Ho^{3+}:$^5I_7$ + Ce^{3+}:$^2F_{7/2}$) [19], this process will increase the number of ions in the Ho^{3+}:$^5I_7$ level. Therefore, for the change in the ions number of Ho^{3+}:$^5I_7$ level, ET and CR are two opposing processes. It is reported that at low doping concentration, the Ce^{3+} can effectively suppress the excited state absorption (ESA) process of Ho^{3+} ions through cross-relaxation process, and low concentration of Ce^{3+} ions does not significantly affect the level lifetime of Ho^{3+}:$^5I_7$ [20]. However, for CeF$_3$ crystals, high concentrations Ce^{3+} ions as a host material produced a stronger deactivation effect than at lower concentrations.

Further study on the energy transfer mechanism of the Ho^{3+}-Ce^{3+}

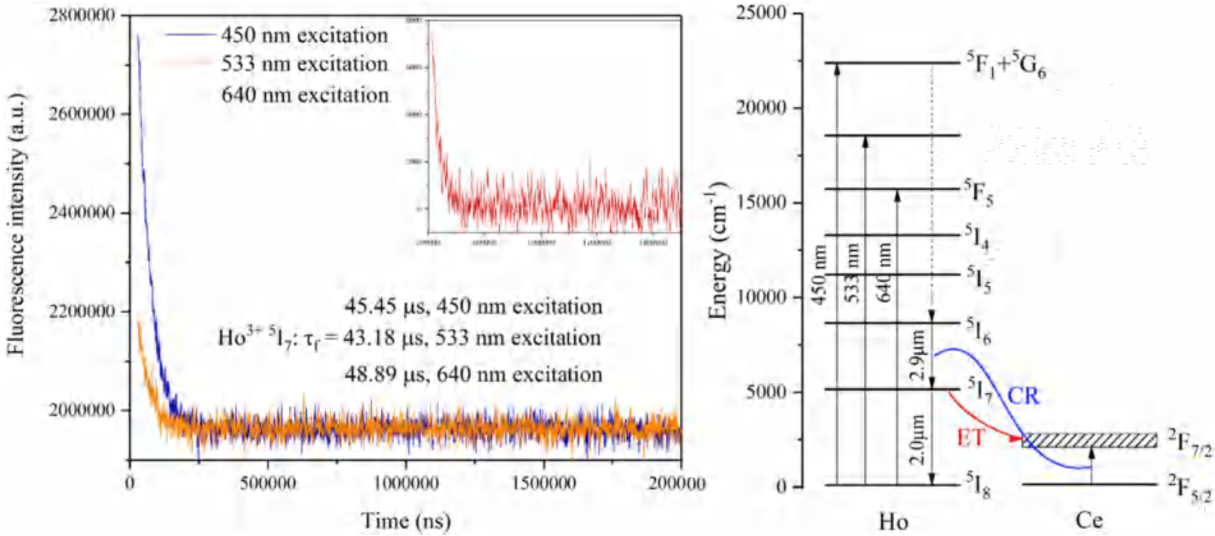

Fig. 6. Fluorescence decay curve of Ho^{3+}:$^5I_7$ level excited by different excitation sources and the energy level scheme of Ho:CeF_3 crystal.

co-doped system requires a measurement of the 2.9 μm emission fluorescence lifetime corresponding to the Ho^{3+}:$^5I_6 \rightarrow {}^5I_7$ transition. But unfortunately, due to the CeF_3 crystal host not transparent in the mid-infrared region, it is very difficult to measure the fluorescence lifetime after 2.3 μm. Therefore, other Ho^{3+}-Ce^{3+} co-doped fluoride crystals are needed to verify the energy transfer process, we are currently studying it in LiYF4 crystals.

For visible light transitions in four-level system like Dy^{3+}:$^4F_{9/2} \rightarrow {}^6H_{13/2}$, the Ce^{3+}:$^4F_{7/2}$ level that is close to the energy of lower laser level can help increase the population inversion level and improve laser efficiency. Perhaps that the Dy^{3+} doped CeF_3 crystal or other highly concentrated Ce^{3+} doped crystals may be a promising material for visible laser applications. Since the ionic radius of La^{3+} ions is similar to that of Ce^{3+} ions, Ce:LaF_3 crystal will be one of the choices.

4. Conclusions

In summary, a Ho^{3+} doped CeF_3 crystal was successfully grown for the first time. The absorption spectrum of this crystal was studied using the J–O theory and the intensity parameters were obtained. The absorption cross-section of peak around 447 nm was 0.43×10^{-20} cm^2, which can be well adapted to commercially available blue laser diode lasers. The stimulated emission cross-section of the $^5I_7 \rightarrow {}^5I_8$ transition were calculated based on the F–L method. The maximum emission cross-section was 0.24×10^{-20} cm^2 at peak around 1988 nm with FWHM of 146 nm. Starting from 2020 nm, the gain cross-section of $^5I_7 \rightarrow {}^5I_8$ transition becomes positive once the population inversion level reaches 20%. Since high concentrations Ce^{3+} ions produced a strong deactivation effect the Ho^{3+}:$^5I_7$ level lifetime is greatly reduced, which has a negative impact on the 2.0 μm mid-infrared emission.

Declaration of Competing Interest

The authors declare that they have no known competing financial interests or personal relationships that could have appeared to influence the work reported in this paper.

Acknowledgment

The experiments were supported by National Key R&D Program of China (No. 2016YFB1102302, No. 2016YFB0701002), National Natural Science Foundation of China (No. 51872307), Equipment Pre-research Foundation Project of China (No. 61409220309).

References

[1] W. Kim, S.R. Bowman, C. Baker, et al., Holmium-doped laser materials for eye-safe solid state laser application, Laser Technol. Defense Security X. Int. Soc. Opt. Photon. 9081 (2014) 908105.
[2] B.M. Walsh, Review of Tm and Ho materials; spectroscopy and lasers, Laser Phys. 19 (4) (2009) 855.
[3] A. Hemming, J. Richards, A. Davidson, et al., 99 W mid-IR operation of a ZGP OPO at 25% duty cycle, Opt. Express 21 (8) (2013) 10062–10069.
[4] X. Yang, B. Yao, Y. Ding, et al., Spectral properties and laser performance of Ho: Sc 2 SiO 5 crystal at room temperature, Opt. Express 21 (26) (2013) 32566–32571.
[5] H.H. Caspers, H.E. Rast, J.L. Fry, Absorption, fluorescence, and energy levels of Ho3+ in LaF3, J. Chem. Phys. 53 (8) (1970) 3208–3216.
[6] K. Ahrens, The magnetoelastic interaction of optical phonons in Ce c La 1− c F 3 single crystals, Zeitschrift für Physik B Condensed Matter 40 (1) (1980) 45–54.
[7] A. Bensalah, K. Shimamura, V. Sudesh, et al., Growth of Tm, Ho-codoped YLiF4 and LuLiF4 single crystals for eye-safe lasers, J. Cryst. Growth 223 (4) (2001) 539–544.
[8] N. Djeu, V.E. Hartwell, A.A. Kaminskii, et al., Room-temperature 3.4-μm Dy: BaYb 2 F 8 laser, Opt. Lett. 22 (13) (1997) 997–999.
[9] M. Pollnau, W. Lüthy, H.P. Weber, et al., Investigation of diode-pumped 2.8-μm laser performance in Er: BaY 2 F 8, Opt. Lett. 21 (1) (1996) 48–50.
[10] S. Li, L. Zhang, M. He, et al., Effective enhancement of 2.87 μm fluorescence via Yb3+ in Ho3+: LaF3 laser crystal, J. Lumin. 203 (2018) 730–734.
[11] R.A. Buchanan, H.E. Rast, H.H. Caspers, Infrared Absorption of Ce3+ in LaF3 and of CeF3, J. Chem. Phys. 44 (11) (1966) 4063–4065.
[12] E.I. Kotova, V.E. Bugrov, M.A. Odnoblyudov, Development of a fiber laser diode module in the spectral range of 445–450 nm with an output optical power of more than 100 W, J. Opt. Technol. 86 (4) (2019) 255–259.
[13] G. Erbert, F. Bugge, J. Fricke, et al., High-power high-efficiency 1150-nm quantum-well laser, IEEE J. Sel. Top. Quantum Electron. 11 (5) (2005) 1217–1222.
[14] H. Zhang, P. Zhou, X. Wang, et al., Hundred-watt-level high power random distributed feedback Raman fiber laser at 1150 nm and its application in mid-infrared laser generation, Opt. Express 23 (13) (2015) 17138–17144.
[15] B.R. Judd, Optical absorption intensities of rare-earth ions, Phys. Rev. 127 (3) (1962) 750.
[16] G.S. Ofelt, Intensities of crystal spectra of rare-earth ions, J. Chem. Phys. 37 (3) (1962) 511–520.
[17] R. Laiho, M. Lakkisto, Investigation of the refractive indices of LaF3, CeF3, PrF3 and NdF3, Philos. Mag. B 48 (2) (1983) 203–207.
[18] W.T. Carnall, P.R. Fields, K. Rajnak, Electronic energy levels in the trivalent lanthanide aquo ions. I. Pr3+, Nd3+, Pm3+, Sm3+, Dy3+, Ho3+, Er3+, and Tm3+, J. Chem. Phys. 49 (10) (1968) 4424–4442.
[19] Y. Qiao, X. Zhou, H. Xia, et al., Enhanced 2.0 μm emission and lowered up-conversion emission in Ce3+/Yb3+/Ho3+ tri-doped Na5Y9F32 single crystals, Opt. Laser Technol. 120 (2019) 105695.
[20] F. Huang, J. Cheng, X. Liu, et al., Ho 3+/Er 3+ doped fluoride glass sensitized by Ce 3+ pumped by 1550 nm LD for efficient 2.0 μm laser applications, Opt. Express 22 (17) (2014) 20924–20935.